Modeled Northern Hemisphere Winter Climate Response to Realistic Siberian Snow Anomalies

GAVIN GONG AND DARA ENTEKHABI

Department of Civil and Environmental Engineering, Massachusetts Institute of Technology, Cambridge, Massachusetts

JUDAH COHEN

Atmospheric and Environmental Research, Inc., Lexington, Massachusetts

(Manuscript received 8 November 2002, in final form 1 May 2003)

ABSTRACT

Wintertime Northern Hemisphere climate variability is investigated using large-ensemble (20) numerical GCM simulations. Control simulations with climatological surface (land and ocean) conditions indicate that the Arctic Oscillation (AO) is an internal mode of the Northern Hemisphere atmosphere, and that it can be triggered through a myriad of perturbations. In this study the role of autumn land surface snow conditions is investigated. Satellite observations of historical autumn–winter snow cover are applied over Siberia as model boundary conditions for two snow-forced experiments, one using the highest observed autumn snow cover extent over Siberia (1976) and another using the lowest extent (1988). The ensemble-mean difference between the two snow-forced experiments is computed to evaluate the climatic response to Siberian snow conditions. Experiment results suggest that Siberian snow conditions exert a modulating influence on the predominant wintertime Northern Hemisphere (AO) mode. Furthermore, an atmospheric teleconnection pathway is identified, involving well-known wave–mean flow interaction processes throughout the troposphere and stratosphere. Anomalously high Siberian snow increases local upward stationary wave flux activity, weakens the stratospheric polar vortex, and causes upper-troposphere stationary waves to refract poleward. These related stationary wave and mean flow anomalies propagate down through the troposphere via a positive feedback, which results in a downward-propagating negative AO anomaly during the winter season from the stratosphere to the surface. This pathway provides a physical explanation for how regional land surface snow anomalies can influence winter climate on a hemispheric scale. The results of this study may potentially lead to improved predictions of the winter AO mode, based on Siberian snow conditions during the preceding autumn.

1. Introduction

Winter climate variability in the extratropical Northern Hemisphere atmosphere is dominated by simultaneous and opposite-signed oscillations of atmospheric mass between mid- and high latitudes. This phenomenon has been extensively studied in recent years, and has been described using various nomenclature, including the North Atlantic Oscillation (NAO; Wallace and Gutzler 1981), the Arctic Oscillation (AO; Thompson and Wallace 1998), and the Northern Annular Mode (NAM; Thompson and Wallace 2001). Although the specific features associated with each term vary, they all describe a set of related atmospheric phenomena. The characteristic oscillations occur in all seasons, but are most prevalent during the winter. For this study the term AO will be used in reference to this general mode of winter climate variability.

A consensus is building within the scientific community that the AO is a fundamental and internal mode of variability in the Northern Hemisphere, but one that may be modulated by various external forcings (Baldwin 2001; Feldstein 2002). This idea is supported by modeling studies with climatological surface (land and ocean) boundary conditions, which nonetheless exhibit the AO mode of variability (Robertson 2001; Gong et al. 2002). Understanding the role played by external forcings, such as anomalies in sea surface temperatures (SSTs), land surface conditions, and the stratosphere, will improve our overall understanding of Northern Hemisphere climate variability. Improved understanding of climate variability is critical to improving climate predictability on seasonal or longer timescales.

In this study the role of land surface snow conditions is investigated, by modeling the wintertime AO response to observation-based snow forcings over Siberia during the autumn–winter season. Siberia has been identified

Corresponding author address: Judah Cohen, Atmospheric and Environmental Research, Inc., 131 Hartwell Ave., Lexington, MA 02421.
E-mail: jcohen@aer.com

in previous studies (Cohen et al. 2001; Gong et al. 2002) as the region with the greatest potential for snow-forced climate modulation. Background on climate modulation by land surface snow is provided in section 2. Section 3 describes the large-ensemble modeling approach used for this study, and section 4 describes the snow-forcing methodology that is employed. The climatic response to snow and corresponding teleconnection pathway are presented in section 5. Finally, conclusions are presented in section 6.

2. Background

The impact of snow on local weather and climate has been extensively studied and is well understood. An inverse relationship generally exists between snow cover and surface air temperature, caused by a change in the surface energy balance due to the presence of snow (Dewey 1977; Foster et al. 1983; Namias 1985; Cess et al. 1991; Cohen and Rind 1991; Leathers and Robinson 1993). The primary mechanism involved is decreased solar radiation due to a higher albedo, but other responsible surface thermodynamic mechanisms include increased thermal emissivity, decreased thermal conductivity, and increased latent heat via snowmelt (McFadden and Ragotzkie 1967; Wagner 1973; Cohen 1994; Walland and Simmons 1996).

The impact of snow on atmospheric dynamics and remote climate has also been studied. Cohen (1994) provides a review of studies in which a climatic response is detected in subsequent seasons and remote regions relative to the snow anomaly. Anomalously high snow cover has been correlated with a delayed springtime surface air temperature rise, reduced 500-mb geopotential height, a weakened Indian summer monsoon, weakened cyclogenesis in eastern North America, and increased spring and summer soil moisture. Most of these studies focus on snow in the late winter season and its impact on subsequent spring and summer climate in regions adjacent to the snow anomaly. Perhaps the most widely studied climatic response is that of the Indian summer monsoon. Numerous observational and modeling studies have consistently reported an inverse relationship between Eurasian winter snow cover and subsequent Indian summer monsoon rainfall (Hahn and Shukla 1976; Barnett et al. 1989; Douville and Royer 1996; Bamzai and Shukla 1999).

The extent and characteristics of land surface snow suggest the potential to influence climate on a much broader scale than has traditionally been investigated. Large, contiguous landmasses compose roughly half of the total surface area in the extratropical Northern Hemisphere. During the autumn–winter season, these landmasses are characterized by extensive snow cover. In addition, snow cover and snow mass exhibits considerable variability in both time and space, especially during the autumn season (Gutzler and Rosen 1992; Robinson et al. 1993).

The breadth of the snow-covered land surface suggests that snow anomalies may influence climate not just on a regional scale, but possibly on a continental or even hemispheric scale. Watanabe and Nitta (1999) investigated the decadal-scale negative to positive AO climate shift that occurred in winter 1989, and suggested that anomalously low Eurasian snow cover anomalies during the preceding autumn may have played a role comparable in magnitude to SST anomalies in amplifying the observed climatic shift. Clark and Serreze (2000) associated snow cover variations in east Asia with winter atmospheric circulation anomalies over the North Pacific. Cohen and Entekhabi (1999) reported a significant interannual correlation of 0.71 between satellite-derived Eurasian autumn snow cover area and the winter AO mode, represented by the first empirical orthogonal function of the observed winter 500-hPa Northern Hemisphere geopotential height field. Cohen and Entekhabi (2001) used a similar approach to establish a significant statistical relationship between interannual winter Eurasian snow cover variations and the winter AO mode. Cohen et al. (2001) performed interannual correlation analyses using gridpoint sea level pressure data, Eurasian autumn snow cover area, and a downward-propagating AO index; they demonstrated that the winter AO may originate as an autumn sea level pressure anomaly over Siberia. Saito et al. (2001) perform an array of diagnostic and statistical analyses to demonstrate that the winter AO may be associated with autumn stationary wave activity flux anomalies over Eurasia.

These observational studies imply but do not conclusively prove a causal relationship between snow and the winter AO, due to competing physical processes and noise inherent in the observed data. Therefore numerical modeling studies are needed to complement the observational studies, by isolating the effect of snow anomalies on winter climate. Unfortunately, relevant modeling studies to date have generally been exploratory in nature. In an early study, Walsh and Ross (1988) perturbed North American and Eurasian snow cover separately for 30-day periods during the late winter. In general they found the large-scale atmospheric circulation to be more sensitive to positive Eurasian snow cover perturbations, with colder air temperatures up to 500 hPa, higher pressure/heights in the Asian Arctic, and lower pressure/heights in the Aleutian region and western Europe. Walland and Simmonds (1997) performed idealized GCM experiments of the January climate response to changes in observed Northern Hemisphere snow cover. They found nonlocal geopotential height and cyclone activity responses over both the North Atlantic and North Pacific basins, and attributed them to local responses over the land surface snow anomalies being swept downstream. Watanabe and Nitta (1998) performed 6-month (September–February) GCM simulations with an artificial low snow perturbation applied to eastern Eurasia. The modeled climatic response re-

sembled the observed winter 1989 climatic shift (i.e., extreme positive AO mode), and was similar to the climatic response of a related GCM simulation forced with observed 1988/1989 SSTs, although the magnitude of the snow-forced response was somewhat smaller. Cohen and Entekhabi (2001) performed a 3-month (Dec–Feb) GCM experiment with an idealized but representative high snow perturbation, which yielded a climatic response resembling a negative AO phase, consistent with observations. Gong et al. (2002) investigated the influence of model-generated interannual snow fluctuations on the winter AO mode. They found that snow variations resulted in a winter AO mode, which was more reminiscent of observations, especially at upper-atmospheric levels, and which originated in Siberia during autumn. These modeling studies are all suggestive of a causal relationship between snow and winter climate, but the idealized conditions that were employed may have led to exaggerated, suppressed, or otherwise unrealistic results.

Another requirement for a complete understanding of the snow–winter climate relationship is a detailed explanation of the physical mechanisms involved, to show that the relationship is real and not a chance or model artifact. Previous studies have hypothesized various potential teleconnection pathways, such as an orographically constrained poleward migration of the semipermanent Siberian high pressure system (Cohen et al. 2001), or a vertical pathway involving upward-propagating stationary wave activity and the stratospheric polar vortex (Saito et al. 2001; Cohen et al. 2002). However, they have not been conclusive in showing that these pathways occur.

We address these issues of realistic forcing and pathway characterization as part of the experimental approach. Rather than using idealized perturbations, snow forcings for this study are derived from visible satellite observations of snow cover. This approach facilitates a meaningful comparison between model results and observed AO mode variability. Another improvement is the use of a large-ensemble modeling approach, in which each snow-forced experiment consists of 20 independent realizations using the same boundary condition. A large ensemble is necessary to distinguish snow-related changes from the naturally occurring interannual variability associated with the AO mode. Finally, model results will be analyzed in detail to identify the precise teleconnection pathways linking the forced-snow anomalies with the climatic response.

3. Large-ensemble, snow-forced GCM experiments

a. Model description and snow parameterization

Numerical simulations are conducted using the Max-Planck Institute for Meteorology ECHAM3 GCM at T42 spectral truncation (roughly 2.8° grid cell resolution). This resolution is adequate for the study of hemispheric-scale atmospheric patterns. Furthermore, at this resolution the model may be used to generate a large ensemble in a computationally affordable manner. ECHAM3 has evolved from the spectral operational weather forecast model used at the European Centre for Medium-Range Weather Forecasts, incorporating physical parameterizations and revised numerical methods appropriate for climate simulations (Roeckner et al. 1992). The land surface parameterization is derived from the Simple Biosphere model (Sellers et al. 1986). Snow is parameterized in a relatively simplistic manner, as described in appendix A. Additional details are provided in DKRZ (1994).

ECHAM3's simulation of snow cover and snow mass compares reasonably well with observations and with other GCMs (Foster et al. 1996; Frei and Robinson 1998). Figure 1a shows the average October snow depth over Eurasia simulated by a 20-yr control simulation of the GCM, designated as CTRL, using monthly climatological sea surface temperature boundary conditions. Model snow water equivalent (SWE) depth is multiplied by ρ_w/ρ_s to convert to snow depth, where $\rho_w = 1000$ kg m^{-3} is used for water density and a typical value of $\rho_s = 300$ kg m^{-3} is used for snow density (DKRZ 1994; Foster et al. 1996). For comparison, the U.S. Air Force Environmental Technical Applications Center (USAF/ETAC) monthly observed global snow depth climatology (Foster and Davy 1988) for October is presented in Fig. 1b. The model appears to replicate the general snow depth features reasonably well, that is, the location of the southern boundary, and separate maxima in northern and eastern Siberia. Snow depths are fairly consistently underestimated throughout Eurasia; this discrepancy has been noted previously in the literature, and attributed in part to deficiencies in the observed data (Foster et al. 1996). Note that snow variability is considerable in October, which presents a challenge to achieving accuracy in both model simulations and observations.

Figure 1c shows plots of monthly average snow-covered area over Eurasia during the autumn–winter season, for the CTRL simulation, the USAF/ETAC snow depth climatology, and National Oceanic and Atmospheric Administration (NOAA) visible satellite snow cover observations (Robinson et al. 1993). All three sources indicate very sparse snow cover in September, a steady increase during autumn and early winter, and peak values in January and February. Once again the CTRL run appears to underestimate the USAF/ETAC observations. At the same time, the CTRL run also slightly overestimates the NOAA observations. This contradiction between the USAF/ETAC and NOAA datasets highlights the shortcomings of snow observations, especially given the general scarcity of data in Siberia and the variable nature of snow in autumn. Overall, the CTRL simulation does a credible job of reproducing the basic observed snow features over Eurasia, and thus serves as a valid platform for conducting snow perturbation experiments.

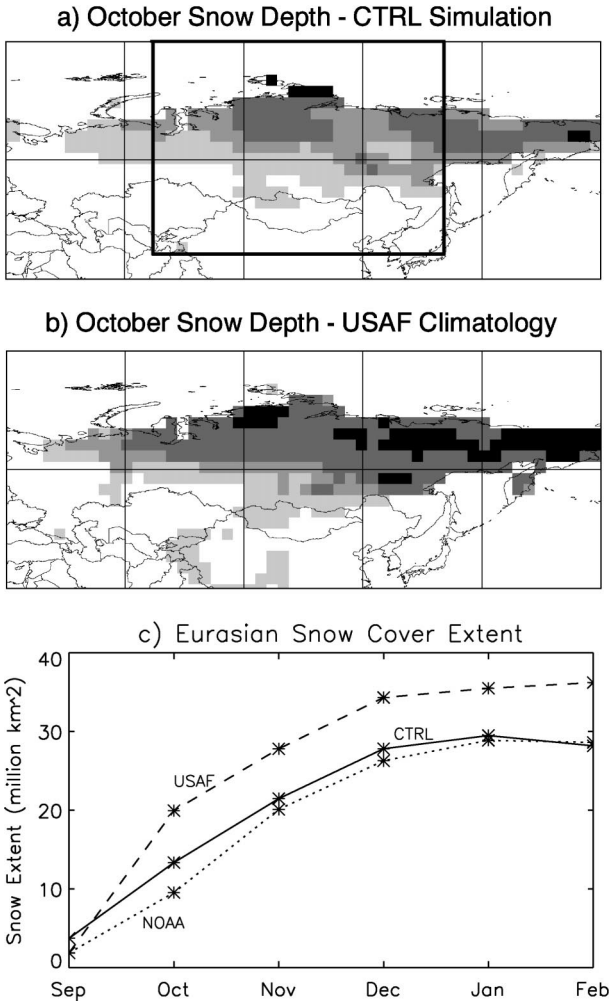

FIG. 1. (a) Average Oct snow depth over Eurasia for the CTRL simulation. Shading represents 1–5 (lightest), 5–10, 10–20, and 20+ cm (darkest). Box indicates Siberia region used for snow-forced boundary conditions during SNO76 and SNO88 experiments. (b) Same as (a) except for USAF–ETAC observed climatology dataset. (c) Monthly average snow cover extent over Eurasia during Sep–Feb for CTRL simulation, USAF/ETAC observations, and NOAA visible satellite observations.

b. Experimental design

The basic experimental design is identical to that described in Gong et al. (2002). The model integration period runs from September to February, to capture the season of greatest snow variability (autumn) and the subsequent (winter) climate response when the AO mode is strongest. Two GCM experiments are performed in this study. In each experiment, grid cell SWE values are prescribed at each model time step, derived from observed weekly snow conditions. One experiment, designated SNO76, uses observations representing extensive snow conditions (September 1976–February 1977), while the other experiment, designated SNO88, uses limited snow conditions (September 1988–February 1989). Section 4 describes the specification of observed snow conditions in greater detail. The prescribed snow mass is then subject to melting and evaporation at each time step, and surface temperatures are allowed to respond accordingly. This minimizes the disruption of surface energy and mass balances that necessarily result from this approach (Gong et al. 2002; also see appendix A).

As stated in section 1, this study focuses on autumn snow anomalies over Siberia as a modulating factor for the subsequent winter AO mode. Therefore, snow is only prescribed over Siberia, specifically land surface grid cells within 36.5°–90.0°N, and 67.5°–140.5°E, as indicated in Fig. 1a. This region exhibits the greatest variability in autumn snow extent between extensive and limited snow years, and thus holds the greatest potential for modulating winter climate. Grid cells outside of this Siberia region are left unaltered, that is, snow is generated and maintained internally by the model. By limiting the snow forcing to a specific targeted region, the climatic response arising from this region can be isolated.

A large ensemble consisting of twenty independent realizations is simulated for each experiment. Recent literature on ensemble GCM integrations suggests that typical studies consisting of six or fewer realizations may be insufficient to distinguish externally forced impacts from internal model variability, especially during the winter when extratropical variability is high. Mehta et al. (2000) use 16 realizations of a 44-yr GCM simulation to illustrate that with increasing ensemble size, the average correlation between modeled and observed NAO indices increases, and the range of correlations over all ensemble set permutations decreases. Gridpoint sea level pressure statistics for our 20-member ensemble experiments similarly exhibit a decreasing range of values over all permutations with increasing ensemble size, with considerably larger variability for ensemble sizes less than ten. Furthermore, the AO is known to exhibit variability at a wide range of timescales, from intraseasonal to interannual or even longer. A large ensemble is needed to fully capture the interannual variability associated with the AO, so that snow-forced differences in the AO mode in excess of the naturally occurring variability can be effectively realized.

Ensemble mean differences between the two experiments are computed as SNO76 − SNO88 (i.e., extensive snow − limited snow), to evaluate the climatic response to a positive snow perturbation over Siberia. Statistical significance of the mean difference between these two 20-member ensembles is determined using the *t* test. Based on previous studies, it is expected that an increase in snow over Siberia will yield a winter climatic response consistent with a negative AO mode. A comprehensive set of diagnostic parameters is evaluated and presented in section 5 to confirm or refute this hypothesis, and to identify the teleconnection pathways that occur.

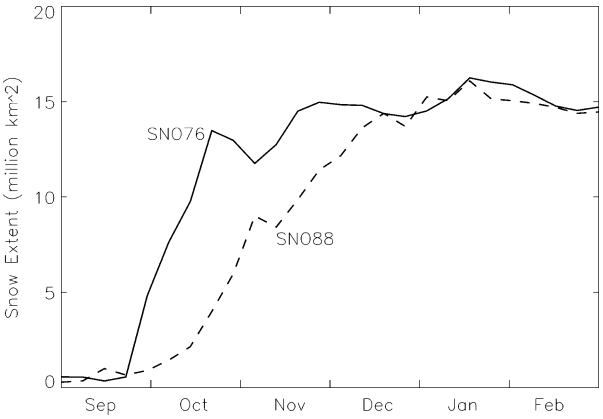

FIG. 2. NOAA visible satellite observations of weekly snow cover extent over Siberia used for the SNO76 (Sep 1976–Feb 1977) and SNO88 (Sep 1988–Feb 1989) experiments.

4. Specification of observed snow conditions

NOAA visible satellite observations of historical autumn–winter snow cover (Robinson et al. 1993) are used as the basis for deriving realistic model boundary conditions for the two Siberian snow-forced experiments. The highest (lowest) observed autumn snow cover over Eurasia occurred in 1976 (1988); therefore the SNO76 (SNO88) experiment uses weekly data from September to February 1976/77 (1988/89). At every time step during the model integration period, Siberian grid cells are specified as snow or no-snow according to each experiment's respective dataset. Thus the two experiments prescribe realistic, observation-based snow cover conditions over Siberia for an extensive snow year (SNO76) and a limited snow year (SNO88).

Figure 2 shows the observed weekly snow cover extent time series over the Siberia forcing region used in the two experiments. Snow cover over Siberia is highly variable during autumn, especially in October when the snow cover extent can vary by roughly a factor of 5. In contrast, during winter variability is minimal since all of Siberia is essentially covered with snow. The large contrast in October highlights the potential for autumn snow anomalies to influence climate.

The NOAA visible satellite observations provide snow cover data, but do not indicate snow depths. It is reasonable to expect extreme seasonal snow conditions to have anomalous snow depths as well as anomalous snow cover exent. Therefore an approximate method is developed for prescribing Siberian snow depth forcings used in the SNO76 and SNO88 experiments. This method is based on the simplifying assumption that if a given location becomes snow-covered earlier (later) than usual, the snowpack will be deeper (shallower) than usual throughout the simulation period. Although this is not necessarily the case, it provides a means of prescribing reasonable and consistent snow depth forcings, derived in part from observed data.

At every Siberian grid cell, the data of initial snow occurrence is determined for the CTRL simulation, and also for the SNO76 and SNO88 snow cover datasets. Next, the weekly SWE time series is assembled for the CTRL simulation. The SWE time series for the SNO76 (SNO88) experiments is then obtained by shifting the CTRL time series backward (forward) in time. The magnitude of the shift is determined by the difference in initial snow occurrence data between SNO76 (SNO88) and CTRL. As a result, the extensive snow experiment consistently exhibits not only broader snow cover but also deeper snow depths than the limited snow experiment, throughout the model integration period. Additional details of this snow depth specification procedure are provided in appendix B.

The resulting Siberian snow boundary conditions are compared to a 25-yr dataset (1966–90) of snow depths in the Former Soviet Union (FSU), observed thricemonthly at over 1300 stations (Krenke 1998). Figure 3 shows a weekly time series of average snow depth over Siberia for the SNO76 and SNO88 experiments (converted from SWE using a typical snow density of 300 kg m^{-3}, see section 3a). Also show are the observed values interpolated from the FSU station data, for each of the 25 yr of historical observations. Note that some regions within the defined Siberia region, such as extreme northern Siberia, Mongolia, and northern China, contain little or no observations and thus may be subject to extrapolation errors. For example, the exceedingly large observed winter snow depth observations in Fig. 3 are due to exaggerated extrapolation of FSU measurements into Mongolia and northern China.

The SNO76 and SNO88 input datasets appear to capture the observed range of average Siberian snow depth reasonably well. Thus the snow cover and snow depth conditions prescribed by the SNO76 and SNO88 experiments reflect realistic cases of positive and negative Siberian snow anomalies, so that the climatic differences that result from the GCM experiments will be representative of realistic Siberian snow forcings. Note that although the difference in winter snow cover extent is minimal between the SNO76 and SNO88 experiments (Fig. 2), the difference in winter snow depth (Fig. 3) is considerable, due to the modeled SWE depth forcing. This provides a potential mechanism by which winter snow anomalies may also modulate winter climate, or at least maintain the modulations initiated by the autumn anomalies.

5. Results

a. Seasonal mean climatic response

The first necessary test is to evaluate the 3-month seasonal mean climatic response over the Northern Hemisphere, in sequential order of known snow cover impact on the atmosphere (i.e., from local thermodynamic to regional and hemispheric dynamical). Figure 4 shows the autumn (SON) and winter (DJF) response

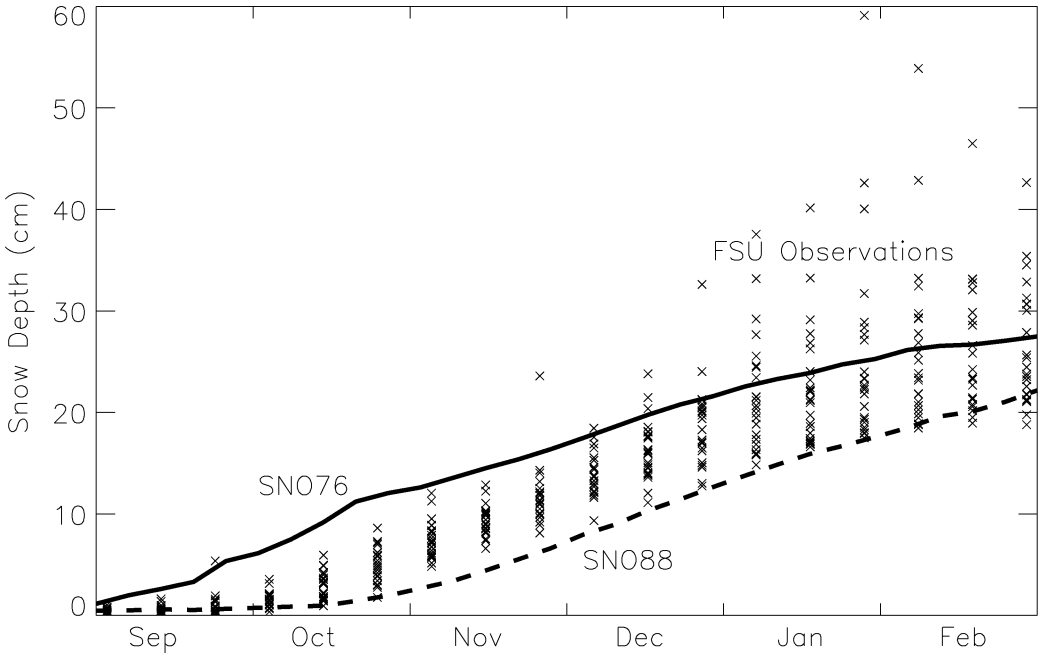

FIG. 3. Weekly average snow depth over Siberia for the SNO76 (solid line) and SNO88 (dashed line) experiments, and for the FSU 25-yr observed point-station snow depth dataset. Each column of crosses represents 25 annual values for each thrice-monthly measurement period.

for surface albedo, surface temperature, and sea level pressure (SLP). The autumn season (Figs. 4a–4c) exhibits the expected local response to positive snow forcing over Siberia, that is, higher surface albedo, lower surface temperature, and higher SLP.

During the winter (Figs. 4d–4f), a notable surface albedo response occurs over Siberia, despite the minimal snow cover forcing indicated in Fig. 2. This is due to the prescribed SWE depth forcing (Fig. 3), and the fact that surface albedo is related to SWE depth in the model snow parameterization (appendix A). The response occurs mainly over southern Siberia (around 45°N), since the surface albedo parameterization is more sensitive to the lower SWE depths that generally reside at lower latitudes. Also important is the fact that solar radiation is more intense over southern Siberia, so that the stronger albedo anomaly translates into a stronger temperature anomaly. As a result, the winter surface temperature and SLP fields also indicate a corresponding local response to snow forcing in southern Siberia.

The winter surface temperature response (Fig. 4e) is not limited to southern Siberia, but rather encompass a broad region extending north and west into the Arctic, northern Europe, and even North America. Other surface thermodynamic mechanisms, for example, increased thermal emissivity and decreased thermal conductivity, may be responsible for the local temperature response in northern Siberia, but they do not explain the remote response outside of the Siberia forcing region. Ongoing research involves additional GCM experiments to identify the precise surface thermodynamic mechanisms associated with snow forcing, and the subsequent remote climate response.

The winter SLP response (Fig. 4f) likewise extends beyond the Siberia forcing region, and encompasses a very broad, hemispheric-scale region, with a large positive anomaly at high latitudes, and large negative anomalies at low latitudes, centered in the North Atlantic and North Pacific basins. The temperature and SLP patterns are both reminiscent of a negative AO mode, and suggest that a positive Siberian snow forcing results in a negative winter AO response. This represents the translation of the local thermodynamic response to a local snow perturbation into a hemispheric dynamical effect.

Figure 4f qualitatively demonstrates that realistic interannual Siberian snow forcings can modulate the hemispheric winter AO mode. Next, this modulation is evaluated quantitatively by developing an unstandardized AO index metric, and assessing the difference in this metric between the SNO76 and SNO88 simulations. The commonly used surface AO index derived from the first empirical orthogonal function (EOF1) of the Northern Hemisphere SLP field (Thompson and Wallace 1998) is a normalized measure, and thus not applicable to assessing changes due to external forcings. A simple AO index is computed here, by subtracting the average SLP north of 61.5°N from the average SLP within the zonal band from 28° to 50°N. These two regions were selected to capture the centers of action in the SLP EOF1 field, and the resulting winter AO index for each experiment is highly correlated ($r = +0.97$ for SNO76;

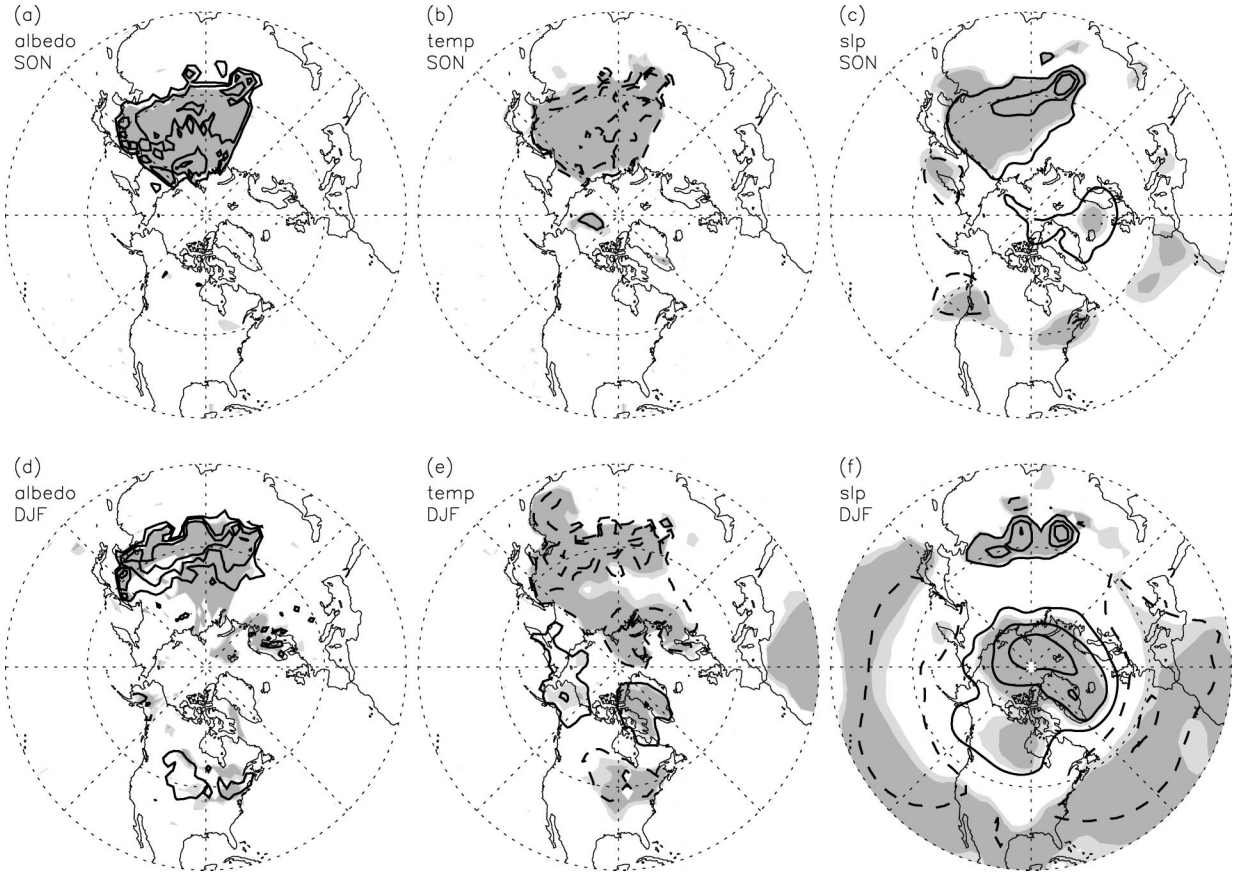

FIG. 4. Surface climatic response to positive Siberian snow forcing (SNO76–SNO88) over the extratropical Northern Hemisphere for (a)–(c) autumn and (d)–(f) winter seasons. (a), (d) Surface albedo contours drawn at ±0.02, 0.1, 0.25. (b), (e) Surface temperature contours drawn at ±1°, 3°, 5°C. (c), (f) Sea level pressure contours drawn at ±1, 3, 5 hPa. Light (dark) shading indicates 90% (95%) statistical significance.

$r = +0.90$ for SNO88) with its respective EOF1-based index.

The resulting ensemble mean winter AO index for SNO76 is roughly 5 hPa less than for SNO88, which is statistically significant at 99%. This exercise was repeated using 500- and 50-hPa geopotential heights, and the resulting AO indices exhibited a snow-forced decrease at 99% and 97% significance, respectively. Thus a positive Siberian snow forcing results in a quantifiable and significant decrease in the winter AO mode throughout the atmosphere.

The model-simulated negative winter AO response to positive Siberian snow anomalies concurs with observational analyses by Cohen and Entekhabi (1999), Cohen et al. (2001), and Saito et al. (2001). Since realistic, observation-based snow forcings are applied in this model study, it is worthwhile to directly compare the modeled winter SLP response in Fig. 4f against the observed response using National Centers for Environmental Prediction (NCEP) reanalysis data (Kalnay et al. 1996) presented in Fig. 3b of Cohen and Entakhabi (1999). The spatial gridpoint correlation coefficient between the two figures is +0.87, which indicates that the modeled spatial response pattern is similar to the observed pattern. However, the spatial standard deviation over gridpoints north of 20°N in Fig. 4f is 2.45 hPa, compared to a value of 8.1 hPa for Cohen and Entekhabi (1999) Fig. 3b. Thus the snow-forced winter AO response pattern is statistically significant and resembles the observed response pattern, but the magnitude of the modeled response is only about 30% that of the observed response.

One potential explanation for the relatively damped model response is that the ECHAM GCM does a poor job of simulating or resolving certain atmospheric features that link Siberian snow anomalies to the winter AO response (see section 6). Teleconnection pathways will be evaluated in detail in sections 5b and 5c. Another potential explanation is that other atmospheric processes occurring in nature act in concert with the positive Siberian snow anomaly, and that these processes are neglected when isolating the climatic response to snow. That the modeled response is weaker but consistent with the observed response supports the notion that snow anomalies serve as an amplifier of the winter AO signal.

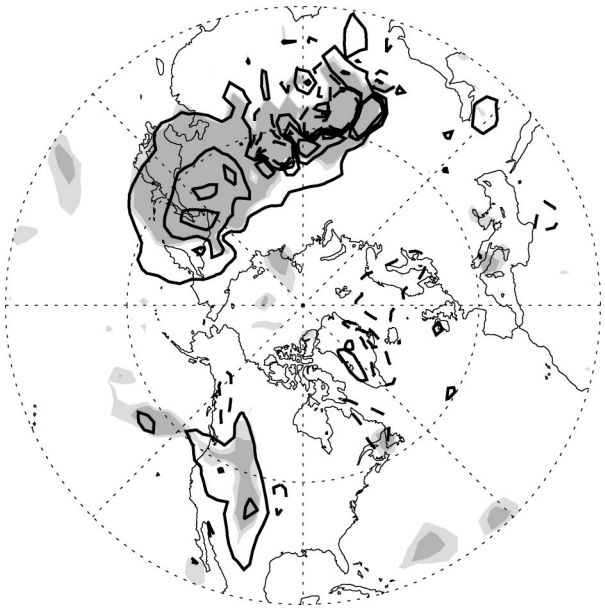

FIG. 5. Vertical wave activity flux response (SNO76–SNO88) at 850-hPa elevation over the extratropical Northern Hemisphere for autumn (SON). Contours drawn at ± 0.01, 0.04, 0.08 $m^2\ s^{-2}$. Light (dark) shading indicates 90% (95%) statistical significance.

b. Vertical wave propagation pathway

A hypothesized teleconnection pathway between the Siberian snow forcing and the hemispheric climate response involves the upward propagation of snow-forced stationary wave activity from the (local) surface to the stratosphere. Saito et al. (2001) and Cohen et al. (2002) describe the general features of this pathway, as they relate to recent literature on the stratospheric forcing of the AO. In this section the manifestation of this pathway in the snow-forced GCM experiments is systematically evaluated, drawing on established wave–mean flow interaction principles as well as recent stratospheric–tropospheric coupling literature. The analysis makes extensive use of the three-dimensional stationary wave activity flux (WAF) diagnostic (Plumb 1985) to describe the transfer of wave energy throughout the atmospheric system. This diagnostic is similar to the classic two-dimensional (zonally averaged) Eliassen–Palm flux (Edmon et al. 1980), but allows for regional analyses by resolving the longitudinal component, at the expense of neglecting transient waves (see section 5c).

Figure 5 shows the vertical WAF response during autumn (SON). The naturally occurring, orographically forced upward wave activity over Siberia (Plumb 1985) increases in response to the positive snow forcing and associated local negative temperature response. Thermal forcings have been shown to amplify orographically forced stationary waves (Ringler and Cook 1999), and observational studies have similarly associated vertical waves with snow (Saito et al. 2001) and temperature (Zhou et al. 2001). Note that the upward WAF anomaly is concentrated in south central and eastern Siberia, which is one of the centers of action for stationary wave activity climatology identified in Plumb (1985).

Figure 6 shows a sequential series of latitude–pressure profile plots, with the WAF response averaged over Siberia longitudes shown as vectors, and the zonal-mean zonal-wind response shown as contours. Each plot represents a 42-day average, centered around the time period shown on the plot. Beginning in early October (Fig. 6a), an upward surface WAF anomaly responds almost immediately to the snow-forced Siberian temperature anomaly. By early November (Fig. 6b) this upward WAF anomaly has propagated into the stratosphere due to prevailing midlatitude tropospheric westerlies (Charney and Drazin 1961), although magnitudes weaken considerably with elevation.

The increased wave activity in the stratosphere weakens the stratospheric polar vortex, as demonstrated in Fig. 6b by the emergence in early November of negative stratospheric zonal-mean zonal-wind anomalies around 60°N. Corresponding positive geopotential height anomalies also occur around 80°N (not shown). Kuroda and Kodera (1999) and Limpasuvan and Hartmann (2000) report similar vortex-related zonal-wind anomalies forced by tropospheric vertical WAF anomalies. Zhou et al. (2001) asserts that the stratosphere is more sensitive to surface-generated wave anomalies than the troposphere, due to its smaller air mass.

The weakened polar vortex causes subsequent upward-tropospheric wave activity (both snow-forced anomalies over Siberia and naturally occurring hemispheric fluxes) to refract poleward, drawn by the negative zonal-wind anomalies at high latitudes. This is evident in early November (Fig. 6b), concurrent with the onset of the weakened vortex in these 42-day average plots. Limpasuvan and Hartmann (2000) and Zhou et al. (2002) report similar meridional wave refraction in the troposphere in response to polar vortex anomalies.

The poleward wave activity flux is associated with equatorward momentum flux (Zhou et al. 2001), which subsequently draws the stratospheric high-latitude zonal-wind and geopotential height anomalies associated with the weakened polar vortex down into the troposphere, and also generates opposite-signed anomalies at midlatitudes. This in turn causes additional poleward and even downward tropospheric wave refraction at lower elevations, and a positive feedback develops in which hemispheric-scale meridional wave activity, zonal wind, and geopotential height anomalies all propagate downward from the stratosphere toward the surface, over the course of a few weeks. Figures 6b–d demonstrate this positive feedback during November, in the form of downward-propagating poleward Siberian WAF anomalies and high-latitude negative zonal-mean zonal-wind anomalies.

The concurrent downward propagation of zonal-wind and meridional wave flux anomalies demonstrated here is consistent with a number of recent studies that de-

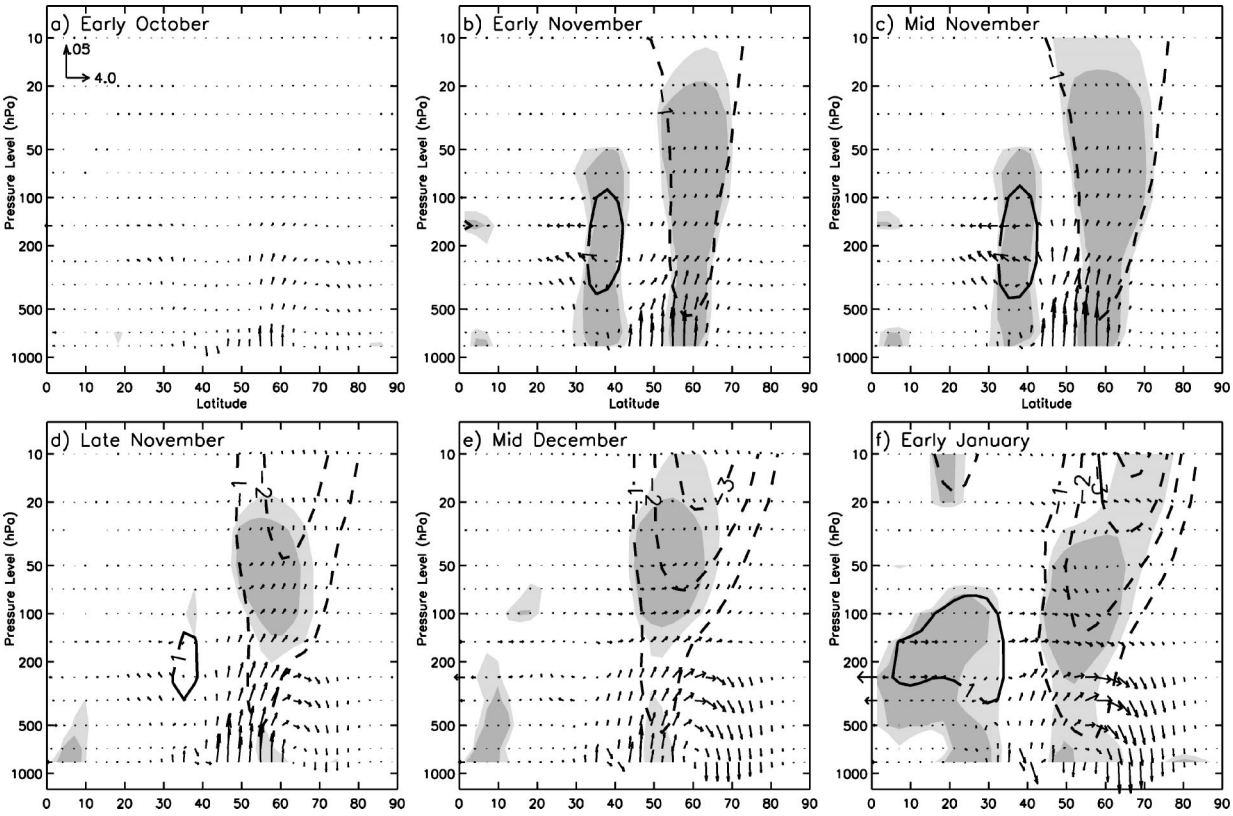

FIG. 6. Latitude (0°–90°N) vs pressure (850–10 hPa) response profiles (SNO76–SNO88) for selected 42-day average periods from early Oct through early Jan. Vectors represent meridional and vertical wave activity flux response averaged over Siberia; (a) scale in $m^2\ s^{-2}$ is indicated. Contours represent zonal-mean zonal wind response; contours drawn at ± 1, 2, 3, 4 m s^{-1}, and light (dark) shading indicates 90% (95%) statistical significance.

scribe stratospheric–tropospheric coupling on a submonthly timescale, and initiated by a stratospheric disturbance (Kuroda and Kodera 1999; Kodera and Kuroda 2000; Baldwin and Dunkerton 1999; Zhou et al. 2002). These studies also suggest that upward-propagating tropospheric waves may trigger the stratospheric disturbance. This study contributes to the discussion by showing that the upward-propagating waves can in turn be caused by snow-forced upward WAF anomalies that originate at the surface and in a localized region, that is, Siberia. The snow cover and corresponding diabatic heating anomalies in this region that produce the upward WAF anomalies are highly variable from year to year.

Once this pathway is initiated in late autumn, it continues into the winter, maintained by the poleward refraction of ambient vertical wave activity. The winter months presented in Figs. 6e–6f indicate gradually increasing meridional WAF anomalies and zonal-wind anomalies, even after the snow-forced upward WAF anomalies over Siberia have dissipated in early January. By midwinter significant dipole zonal-mean zonal-wind (Fig. 6f) and geopotential height (not shown) anomalies have propagated down to the surface. This pattern is indicative of the negative winter AO mode presented in Fig. 4f, and thereby completes the atmospheric teleconnection pathway linking Siberian snow anomalies to the winter AO mode via vertical stationary wave propagation and stratospheric–tropospheric coupling.

Additional analyses are now presented to portray specific features and thereby provide a more comprehensive description of the overall teleconnection. In Fig. 6, the poleward wave refraction and downward mean flow propagation appears to occur more or less continuously from late autumn through winter. This is in part due to the 42-day averaging that is used, which masks short-term fluctuations in order to present a smoothed, generalized response pattern. Applying weekly averaging instead reveals that in fact the submonthly scale teleconnection pathway occurs in distinct pulses. Figure 7 shows plots that are similar to Fig. 6, except that weekly averages are computed instead of 42-day averages. Figures 7a–7c show one pulse during a 3-week sequence in October, and Figs. 7d–7f show a second pulse during a 3-week sequence in December. At the beginning of each sequence (Figs. 7a,d), no Siberian snow-forced upward WAF anomalies or zonal-mean zonal-wind anomalies are apparent. The poleward and downward WAF anomalies in Fig. 7d likely represent the latter stages of a preceding pulse. During the second week (Figs. 7b,e), a strong Siberian upward WAF anomaly originates at

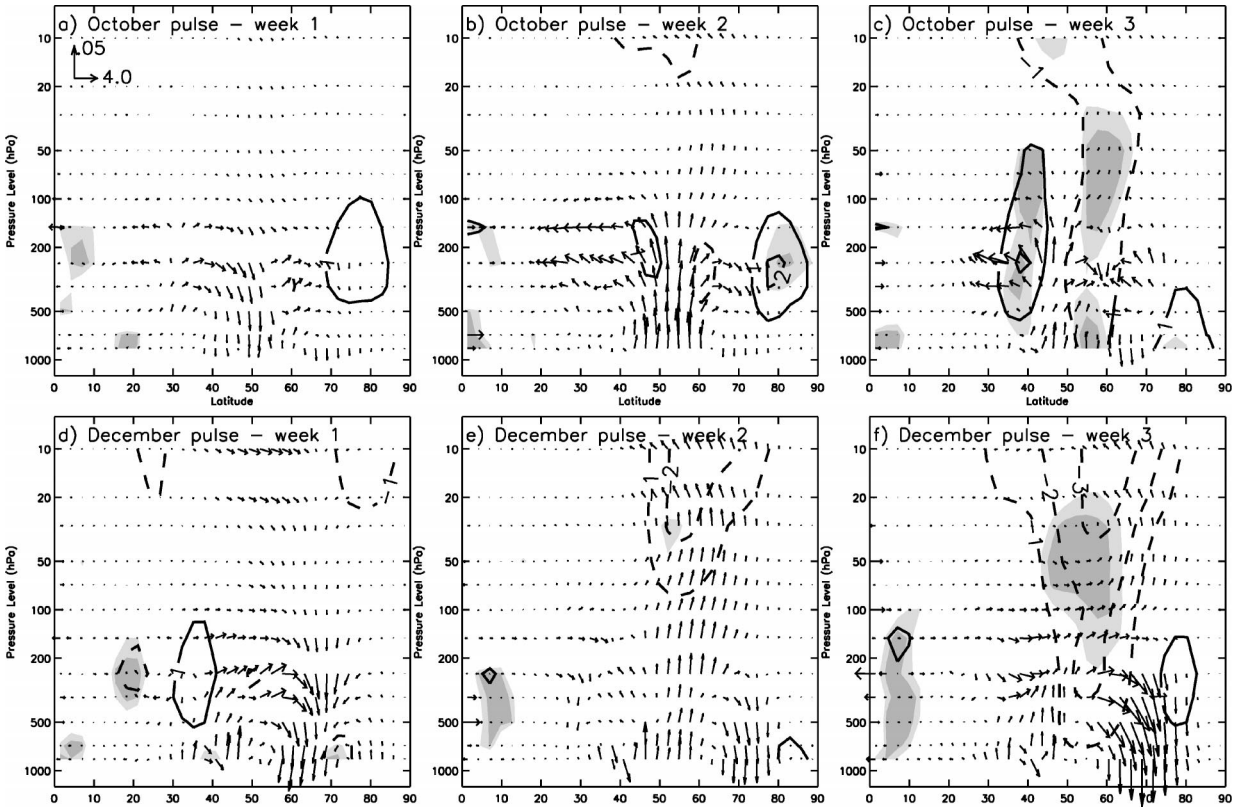

FIG. 7. Same as for Fig. 6 except for selected sequential 1-week average periods in (a)–(c) Oct, and (d)–(f) Dec.

the surface and is maintained throughout the troposphere and well into the stratosphere, whereas the temporally smoothed plots in Fig. 6 showed substantial weakening of the anomaly with elevation. Also, initial stratospheric zonal-wind anomalies associated with the weakened vortex begin to appear. The third week in each sequence (Figs. 7c,f) no longer exhibits a strong upward WAF anomaly, but does show clear downward propagating zonal-wind anomalies. The December pulse (Fig. 7f) exhibits a clear poleward and downward WAF propagation, while this response is less clear for the initial, early season October pulse (Fig. 7c).

Thus for each pulse, a rapid upward WAF anomaly is followed by downward propagating mean-flow anomalies, which dissipate after a few weeks, and another pulse begins soon after. The initial teleconnection pulse in mid-October is almost certainly caused by the initial October snow-forcing anomaly (Fig. 2). Subsequent pulses may be due to other large anomaly periods in the observation-based snow boundary condition. Winter pulses may also be due to the increase in wave activity that naturally occurs in the winter months, which amplify the snow-forced WAF anomaly. The short timescale of the teleconnection pulses suggests that an AO type response may be noticeable as early as late October, following the initial October WAF anomaly pulse (Figs. 7a–7c). Subsequent pulses gradually strengthen the AO signal, until it becomes apparent during the winter months in Figs. 4 and 6.

An important facet of this teleconnection pathway is the ability of a regional surface snow forcing over Siberia to generate a hemispheric-scale winter AO response. This occurs because the regional upward WAF anomaly over Siberia is strong enough (in climatology) to propagate to the stratosphere and weaken the polar vortex, which is a hemispheric phenomenon. This weakened vortex is then able to draw refracted stationary waves throughout the Northern Hemisphere, not just over Siberia. Figure 8 shows snow-forced horizontal WAF anomaly vectors in the upper troposphere (250 hPa) during winter (DJF). Poleward refraction can be seen throughout the Northern Hemisphere at mid to high latitudes. As a result, the downward propagation of mean-flow anomalies is hemispheric in scale, which yields the AO-type winter climatic response.

The downward-propagating mean flow anomalies suggest that the AO mode likewise propagates downward from the stratosphere to the surface. In section 5a, an unstandardized winter (DJF) AO index metric was developed in order to evaluate its response to Siberian snow forcing. Figure 9 presents the SNO76–SNO88 difference in this index, computed and normalized over 12 different atmospheric levels from 1000 to 10 hPa, on a 42-day rolling average basis over the September–Feb-

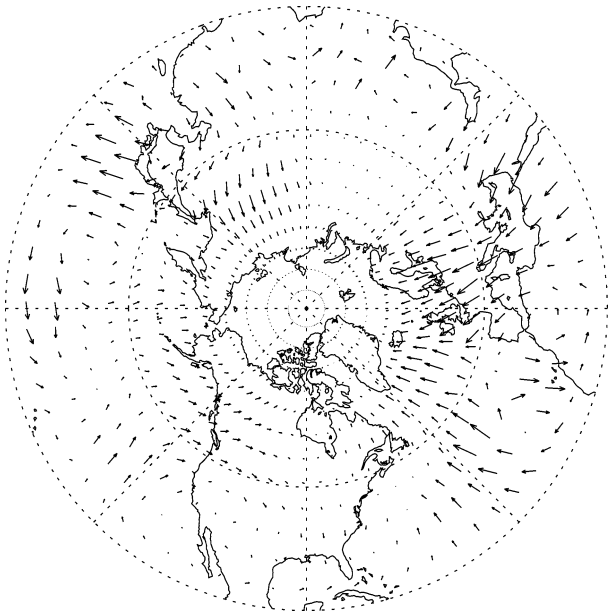

FIG. 8. Horizontal wave activity flux response (SNO76–SNO88) at 250-hPa elevation over the extratropical Northern Hemisphere for winter (DJF). Largest vector drawn represents 9 m^2 s^{-2}.

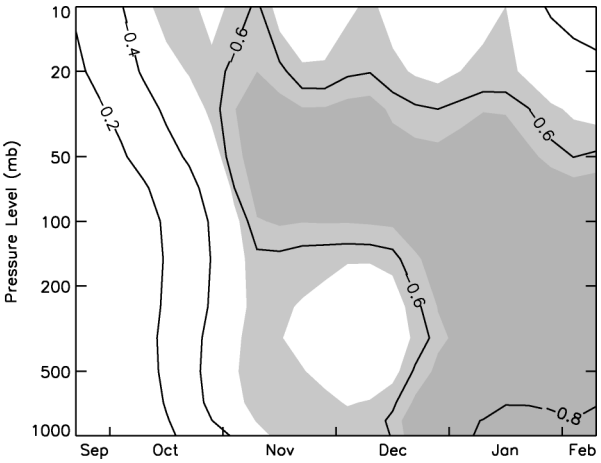

FIG. 9. Weekly evolution (horizontal axis) over the atmospheric column (vertical axis) of normalized 42-day rolling average hemispheric AO index response (SNO76–SNO88). Contours drawn at -2, -4, -6, -8 std dev. Light (dark) shading indicates 90% (95%) statistical significance.

ruary model integration period. A negative AO index anomaly first appears in the late autumn stratosphere, indicative of a weakened polar vortex. A rapid but weak downward propagation to the surface occurs during November, consistent with the submonthly timescale of the vertical teleconnection pathway. Stronger and more significant AO index anomalies remain in the stratosphere until late December, before propagating down to the surface during the remainder of the winter season. This AO propagation pattern is consistent with the temporally smoothed mean flow anomalies depicted in Fig. 6. Baldwin and Dunkerton (1999) use observed data to detect a similar downward-propagating winter AO signal originating in the stratosphere. Although realistic snow anomalies over Siberia begin producing rapidly propagating mean flow anomaly pulses during autumn, the strongest AO mode modulations arising from these pulses do not effectively propagate down to the surface until winter.

c. Stationary versus transient waves

As noted in section 5b, the WAF diagnostic used in Figs. 5–8 is limited to stationary waves. Although stationary wave activity is usually the dominant feature involved in climate variability (Limpasuvan and Hartmann 2000), it is possible that the neglect of transient waves may obscure other important facets of the snow-forced vertical wave mean flow teleconnection pathway. Therefore, the classic two-dimensional, zonally averaged Eliassen–Palm (EP) flux is computed, to evaluate the relative contribution of stationary and transient waves.

Figure 10a shows the snow-forced vertical EP flux response at 500 hPa for October. Also presented are the stationary and transient components that compose the total EP flux. The large upward (positive) anomaly centered around 57°N is the direct response to forcing by Siberian snow, and the figure shows that stationary waves dominate the total wave flux response. Figure 10b similarly shows meridional EP flux response at 500 hPa for January. A broad poleward (positive) anomaly occurs at midlatitudes, representing the poleward refraction of wave activity that occurs in response to a weakened polar vortex. Once again stationary waves dominate where there is a peak in the total wave flux response. For two key tropospheric facets of the snow-forced vertical wave mean flow teleconnection pathway, the climatic response of transient waves is shown to be relatively small compared to that of stationary waves. Therefore we can conclude that the stationary WAF diagnostic is an appropriate metric for diagnosing the planetary wave and overall atmospheric teleconnection response to Siberian snow anomalies.

6. Conclusions

Recent studies (see section 2) have introduced the idea that interannual land surface snow perturbations can be substantial enough to exert a modulating influence on the AO mode of variability. Observational studies have indicated statistically significant correlations between Eurasian snow cover and winter AO mode indices, and idealized GCM experiments have suggested a causal relationship between snow and winter climate. Several atmospheric teleconnection pathways have also been hypothesized, though not fully evaluated. This study builds upon these ideas by conducting large-ensemble GCM simulations of autumn–winter climate, to

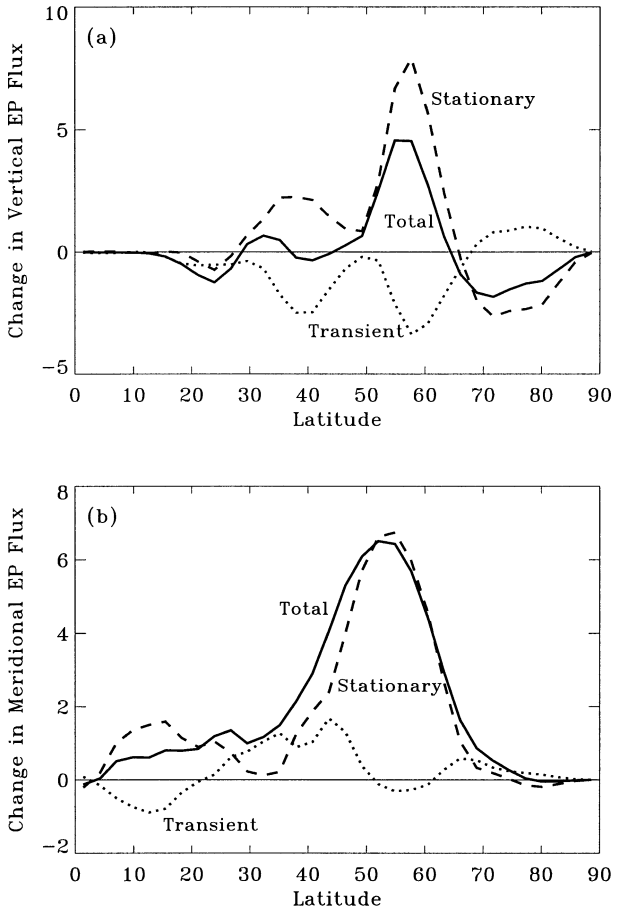

FIG. 10. Eliassen–Palm flux response (SNO76–SNO88) at 500-hPa elevation over Northern Hemisphere latitudes, including stationary and transient components. (a) Vertical flux response for Oct (10^{16} hPa m^3). (b) Meridional flux response for Jan (10^{13} m^3). Zero flux response line also included for reference.

fully evaluate the winter climatic response to realistic, observation-based snow forcings over Siberia.

This study improves upon previous idealized GCM studies in a number of ways. First, realistic, observation-based snow boundary conditions are developed and applied, based upon historical visible satellite data. This helps to ensure that the modeled climatic response to snow is reasonable and applicable to the observed climatic response. Second, a large-ensemble modeling approach consisting of 20 independent realizations is employed, to distinguish snow-forced modulations of the AO mode from the naturally occurring interannual variability associated with the AO mode. Third, the snow forcing is limited to Siberia, a region that has been argued to be the most important for snow-forced winter climate modulation. Last, the physical mechanisms and atmospheric teleconnection pathways linking the forced-snow anomalies with the climatic response are evaluated in detail.

Three-month seasonal mean analyses over the Northern Hemisphere indicate a clear and significant negative AO anomaly during the winter (DJF), resulting from positive Siberian snow forcings and associated local climatic responses, which occur primarily in autumn (SON). The spatial pattern of the snow-forced climatic response is well correlated with observations (+0.87), but the magnitude of the response is only about 30% as large as the observed response. An unstandardized AO index has also been developed, which indicates a statistically significant decrease at various atmospheric levels due to variability in snow cover and snow depth.

A teleconnection pathway involving the vertical propagation of stationary wave activity is investigated. Drawing on established wave–mean flow interaction theory and recent studies involving stratospheric–tropospheric coupling, a detailed pathway has been developed that describes the physical mechanisms by which regional-scale snow anomalies over Siberia result in hemispheric-scale AO mode modulations. Anomalously high Siberian snow increases local upward stationary wave flux activity, weakens the stratospheric polar vortex, and causes upper-tropospheric stationary waves to refract poleward. These related stationary wave and mean flow anomalies propagate down through the troposphere via a positive feedback, over the course of a few weeks. This anomaly pathway occurs in several distinct pulses from midautumn through winter, maintained in part by naturally occurring upward wave activity during the winter. The net result is a gradual downward propagation of a negative AO anomaly during the winter season from the stratosphere to the surface.

The modeled climatic response underestimates the observed climatic response, but this may be due in part to limitations associated with the ECHAM3 GCM. A critical component of the vertical teleconnection pathway involves the propagation of stationary wave activity into the stratosphere, and subsequent weakening of the polar vortex. However, the stratosphere is poorly resolved in ECHAM3, with only four of its nineteen vertical layers centered above 100 hPa, and only seven layers above 200 hPa. The poor stratospheric resolution may inhibit the vortex anomalies that occur in response to Siberian snow forcings, which subsequently may inhibit the downward-propagating hemispheric mean flow anomalies that make up AO mode response. A GCM with a fully resolved stratosphere may produce larger snow-forced AO mode anomalies that are closer in magnitude to observations. This is the subject of follow-up experiments to this study.

This modeling study clearly demonstrates that realistic snow forcings over Siberia have the capability to exert a modulating influence on the winter AO mode of variability. The results are consistent with previous studies suggesting that positive snow anomalies lead to a negative AO response. Identifying the vertical wave propagation teleconnection pathway by which this modulation can occur underscores the validity of the modeled snow–climate relationship. Therefore interannual land surface snow anomalies over Siberia should be

recognized as a potentially important contributor to winter Northern Hemisphere climate variability. A full understanding of this relationship, and its incorporation into climate prediction algorithms, may help to improve climate predictability on seasonal or longer timescales.

Acknowledgments. This investigation was supported by National Science Foundation Grants ATM-9902433 and ATM-0127667. We would like to thank two anonymous reviewers and Dr. Judith Perlwitz for their insightful comments. We would like to thank Dr. David Robinson for his assistance with the NOAA visible satellite snow cover data.

APPENDIX A

ECHAM3 GCM Snow Parameterization

Snow depth in the ECHAM3 GCM is maintained at each grid cell as an internal state variable S, in the form of snow water equivalent. A distinct snowpack layer resides above the surface soil layers, and evolves according to a budget equation:

$$\frac{\partial}{\partial t}S = \frac{J_S + P_S - M_S}{\rho_w}, \tag{A.1}$$

where J_S = evaporation rate over the snowpack, P_S = snowfall rate over the snowpack, M_S = snowmelt rate over the snowpack, and ρ_w = density of water. For snow depths greater than 0.025 m SWE, snowpack temperature T_S evolves via a separate heat conduction equation for the snowpack:

$$\frac{\partial}{\partial t}T_S = \frac{F}{\rho_S C_S S}, \tag{A.2}$$

where F = sum of radiative and turbulent fluxes at the surface, ρ_S = snow density, and C_S = heat capacity of snow. For snow depths less than 0.025 m SWE, T_S is not updated, and the basic surface heat conduction equation is solved irrespective of the snowpack. Surface albedo α_{surf} is related to the snow depth via

$$\alpha_{\text{surf}} = \alpha_b + (\alpha_S - \alpha_b)\frac{S}{S + S^*}, \tag{A.3}$$

where α_b = surface background albedo, α_S = snow albedo, and S^* = 0.01 m SWE. Finally, the snow-covered grid cell fraction F_S is parameterized as

$$F_S = \min\left(1, \frac{S}{S_c}\right), \tag{A.4}$$

where S_c = 0.015 m SWE. For the SNO76 and SNO88 experiments, the prescribed snow depths are subject to the above parameterization equations at each model time step. However the snow depth is not updated, but rather prescribed again at each subsequent time step.

APPENDIX B

Specification of Snow Depth Conditions

Prescribing realistic weekly snow depths presents a challenge, since reliable and comprehensive historical snow depth data are not readily available. Yet their inclusion in the model boundary conditions is desirable, since snow depths can vary considerably over Siberia (see Fig. 1), and some of the mechanisms known to affect local climate (e.g., thermal emissivity and thermal conductivity) vary with snow depth. A 25-yr dataset (1966–90) of observed station snow depths in the Former Soviet Union is available (Krenke 1998), but coverage is too sparse over the modeled Siberia forcing region to be used as the basis for spatial interpolation and gridpoint snow depth input. Therefore, an approximate method is developed for prescribing grid cell Siberian SWE depths associated with the observed snow cover used in the SNO76 and SNO88 experiments. The basic methodology has been described in section 4; this appendix provides additional details related to the snow depth specification procedure.

The temporal translation of the weekly CTRL SWE time series is controlled by the initial snow occurrence dates for SNO76 and SNO88, relative to that for CTRL. This translation can be expressed as

$$S_{76}(t) = S_{\text{CT}}(t + \Delta t_{76}); \qquad \Delta t_{76} = t^*_{\text{CT}} - t^*_{76} \tag{B.1}$$

$$S_{88}(t) = S_{\text{CT}}(t - \Delta t_{88}); \qquad \Delta t_{88} = t^*_{88} - t^*_{\text{CT}}, \tag{B.2}$$

where S_{76} = SWE depth for SNO76, S_{88} = SWE depth for SNO88, S_{CT} = SWE depth for CTRL, t = time during model integration period, t^*_{76} = initial snow date for SNO76, t^*_{88} = initial snow date for SNO88, and t^*_{CT} = initial snow date for CTRL. The observed snow cover datasets for the two perturbation experiments represent extreme early and late autumn snow cover, so that generally $t^*_{76} < t^*_{\text{CT}} < t^*_{88}$, and hence $S_{88} < S_{\text{CT}} < S_{76}$ at all t. Also, the magnitude of the SWE variation is directly proportional to the magnitude of the difference in initial snow dates.

The snow specification datasets were checked and adjusted as needed to ensure that the SNO76 (SNO88) boundary condition always exhibits more (less) extensive snow cover, earlier (later) initial snow occurrence, and larger (smaller) SWE values over Siberia, relative to the CTRL run, thereby representing a positive (negative) snow perturbation. Furthermore, a minimum SWE value of 4.0 cm was applied to the SNO76 Siberian boundary condition, in order to maximize the surface thermodynamic contrast between the two experiments. The 4.0 cm SWE exceeds the critical thresholds for maximum snow impact on the surface energy balance in the ECHAM3 GCM land surface parameterization described in appendix A.

REFERENCES

Baldwin, M. P., 2001: Annular modes in global daily surface pressure. *Geophys. Res. Lett.,* **28,** 4115–4118.

——, and T. J. Dunkerton, 1999: Propagation of the Arctic Oscillation from the stratosphere to the troposphere. *J. Geophys. Res.,* **104** (D24), 30 937–30 946.

Bamzai, A. S., and J. Shukla, 1999: Relation between Eurasian snow cover, snow depth, and the Indian summer monsoon: An observational study. *J. Climate,* **12,** 3117–3132.

Barnett, T. P., L. Dumenil, U. Schlese, E. Roeckner, and M. Latif, 1989: The effect of Eurasian snow cover on regional and global climate variations. *J. Atmos. Sci.,* **46,** 661–685.

Cess, R. D., and Coauthors, 1991: Interpretation of snow-climate feedback as produced by 17 general circulation models. *Science,* **253,** 888–892.

Charney, J. G., and P. G. Drazin, 1961: Propagation of planetary scale disturbances from the lower into the upper atmosphere. *J. Geophys. Res.,* **66,** 83–109.

Clark, M. P., and M. C. Serreze, 2000: Effects of variations in east Asian snow cover on modulating atmospheric circulation over the North Pacific Ocean. *J. Climate,* **13,** 3700–3710.

Cohen, J., 1994: Snow cover and climate. *Weather,* **49,** 150–156.

——, and D. Rind, 1991: The effect of snow cover on climate. *J. Climate,* **4,** 689–706.

——, and D. Entekhabi, 1999: Eurasian snow cover variability and Northern Hemisphere climate predictability. *Geophys. Res. Lett.,* **26,** 345–348.

——, and ——, 2001: The influence of snow cover on Northern Hemisphere climate variability. *Atmos.–Ocean,* **39,** 35–53.

——, K. Saito, and D. Entekhabi, 2001: The role of the Siberian High in Northern Hemisphere climate variability. *Geophys. Res. Lett.,* **28,** 299–302.

——, D. Salstein, and K. Saito, 2002: A dynamical framework to understand and predict the major Northern Hemisphere climate mode. *Geophys. Res. Lett.,* **29,** 1412, doi:10.1029/2001GL014117.

Dewey, K. F., 1977: Daily maximum and minimum temperature forecasts and the influence of snow cover. *Mon. Wea. Rev.,* **105,** 1594–1597.

DKRZ, 1994: The ECHAM3 Atmospheric General Circulation Model. Deutsches Klimarechenzentrum Tech. Rep. 6, 182 pp.

Douville, H., and J.-F. Royer, 1996: Sensitivity of the Asian summer monsoon to anomalous Eurasian snow cover within the Meteo-France GCM. *Climate Dyn.,* **12,** 449–466.

Edmon, H. J., Jr., B. J. Hoskins, and M. E. McIntyre, 1980: Eliassen–Palm cross sections for the troposphere. *J. Atmos. Sci.,* **37,** 2600–2616.

Feldstein, S. B., 2002: The recent trend and variance increase of the annular mode. *J. Climate,* **15,** 88–94.

Foster, D. J., Jr., and R. D. Davy, 1988: Global snow depth climatology. USAF Environmental Technical Applications Center Rep. USAFETAC/TN-88/006, 48 pp.

Foster, J., M. Owe, and A. Rango, 1983: Snow cover and temperature relationships in North America and Eurasia. *J. Climate Appl. Meteor.,* **22,** 460–469.

——, and Coauthors, 1996: Snow cover and snow mass intercomparisons of general circulation models and remotely sensed datasets. *J. Climate,* **9,** 409–426.

Frei, A., and D. A. Robinson, 1998: Evaluation of snow extent and its variability in the atmospheric model intercomparison project. *J. Geophys. Res.,* **103** (D8), 8859–8871.

Gong, G., D. Entekhabi, and J. Cohen, 2002: A large-ensemble model study of the wintertime AO–NAO and the role of interannual snow perturbations. *J. Climate,* **15,** 3488–3499.

Gutzler, D. S., and R. D. Rosen, 1992: Interannual variability of wintertime snowcover across the Northern Hemisphere. *J. Climate,* **5,** 1441–1447.

Hahn, D. G., and J. Shukla, 1976: An apparent relationship between the Eurasian snow cover and Indian monsoon rainfall. *J. Atmos. Sci.,* **33,** 2461–2462.

Kalnay, E., and Coauthors, 1996: The NCEP/NCAR 40-Year Reanalysis Project. *Bull. Amer. Meteor. Soc.,* **77,** 437–471.

Kodera, K., and Y. Kuroda, 2000: Tropospheric and stratospheric aspects of the Arctic Oscillation. *Geophys. Res. Lett.,* **27,** 3349–3352.

Krenke, A., cited 1998: Former Soviet Union hydrological snow surveys. National Snow and Ice Data Center/World Data Center for Glaciology, Boulder, Co. [Available online at http://nsidc.org/data/docs/noaa/g01170_fsu_snow/.]

Kuroda, Y., and K. Kodera, 1999: Role pf planetary waves in stratosphere–troposphere coupled variability in the Northern Hemisphere winter. *Geophys. Res. Lett.,* **26,** 2375–2378.

Leathers, D. J., and D. A. Robinson, 1993: The association between extremes in North American snow cover extent and United States temperature. *J. Climate,* **6,** 1345–1355.

Limpasuvan, V., and D. L. Hartmann, 2000: Wave-maintained annular modes of climate variability. *J. Climate,* **13,** 4414–4429.

Mehta, V. M., M. J. Suarez, J. Manganello, and T. L. Delworth, 2000: Predictability of multiyear to decadal variations in the North Atlantic Oscillation and associated Northern Hemisphere climate variations. *Geophys. Res. Lett.,* **27,** 121–124.

McFadden, J. D., and R. A. Ragotzkie, 1967: Climatological significance of albedo in central Canada. *J. Geophys. Res.,* **72,** 1135–1143.

Namias, J., 1985: Some empirical evidence for the influence of snow cover on temperature and precipitation. *Mon. Wea. Rev.,* **113,** 1542–1553.

Plumb, R. A., 1985: On the three-dimensional propagation of stationary waves. *J. Atmos. Sci.,* **42,** 217–229.

Ringler, T. D., and K. H. Cook, 1999: Understanding the seasonality of orographically forced waves: Interaction between mechanical and thermal forcing. *J. Atmos. Sci.,* **56,** 1154–1174.

Robertson, A. W., 2001: Influence of ocean–atmosphere interaction on the Arctic Oscillation in two general circulation models. *J. Climate,* **14,** 3240–3254.

Robinson, D. A., K. F. Dewey, and R. R. Heim Jr., 1993: Global snow cover monitoring: An update. *Bull. Amer. Meteor. Soc.,* **74,** 1689–1696.

Roeckner, E., and Coauthors, 1992: Simulation of the present-day climate with the ECHAM model: Impact of model physics and resolution. Max-Planck-Institute for Meteorology Rep. 93, Hamburg, Germany, 171 pp.

Saito, K., J. Cohen, and D. Entekhabi, 2001: Evolution of atmospheric response to early-season Eurasian snow cover anomalies. *Mon. Wea. Rev.,* **129,** 2746–2760.

Sellers, P. J., Y. Mintz, Y. C. Sud, and A. Dalcher, 1986: A simple biosphere model (Sib) for use within general circulation models. *J. Atmos. Sci.,* **43,** 505–531.

Thompson, D. W. J., and J. M. Wallace, 1998: The Arctic Oscillation signature in wintertime geopotential height and temperature fields. *Geophys. Res. Lett.,* **25,** 1297–1300.

——, and ——, 2001: Regional climate impacts of the Northern Hemisphere annular mode. *Science,* **293,** 85–89.

Wagner, A. J., 1973: The influence of average snow depth on monthly mean temperature anomaly. *Mon. Wea. Rev.,* **101,** 624–626.

Wallace, J. M., and D. S. Gutzler, 1981: Teleconnections in the geopotential height field during the Northern Hemisphere winter. *Mon. Wea. Rev.,* **109,** 784–812.

Walland, D. J., and I. Simmonds, 1996: Sub-grid scale topography and the simulation of Northern Hemisphere snow cover. *Int. J. Climatol.,* **16,** 961–982.

——, and ——, 1997: Modelled atmospheric response to changes in Northern Hemisphere snow cover. *Climate Dyn.,* **13,** 25–34.

Walsh, J. E., and B. Ross, 1988: Sensitivity of 30-day dynamical forecasts to continental snow cover. *J. Climate,* **1,** 739–754.

Watanabe, M., and T. Nitta, 1998: Relative impacts of snow and sea surface temperature anomalies on an extreme phase in the winter atmospheric circulation. *J. Climate,* **11,** 2837–2857.

——, and ——, 1999: Decadal changes in the atmospheric circulation and associated surface climate variations in the Northern Hemisphere winter. *J. Climate,* **12,** 494–509.

Zhou, S., A. J. Miller, J. Wang, and J. K. Angell, 2001: Trends of NAO and AO and their associations with stratospheric processes. *Geophys. Res. Lett.,* **28,** 4107–4110.

——, ——, ——, and ——, 2002: Downward-propagating temperature anomalies in the preconditioned polar stratosphere. *J. Climate*, **15,** 781–792.